positions could be experimentally determined.[21]

Conclusions

The analysis of the diffraction data show conclusively that in aqueous erbium halide and perchlorate solutions the metal ion is coordinated by eight water molecules with an Er–H_2O distance of 2.35 Å. This is independent of concentration and of anion in the solutions investigated. Inner-sphere complexes are formed only at very high ligand concentration and then only to a small extent. The Er–Cl distances in these ion pairs do not differ significantly from corresponding distances in known crystal structures.[26]

The erbium ion also has a well-defined second coordination sphere containing both water molecules and anions, with Er–H_2O distances of about 4.50 Å. The Er–Cl and Er–Br distances in these solvent-separated ion pairs are about 5.0 Å and are not significantly different although the Br^- ionic radius is larger than that of Cl^-. This might be caused by the difference in the ability of Cl^- and of Br^- to form hydrogen bonds. In a preliminary investigation of an iodide solution the corresponding Er–I distance is found to be 5.25 Å. The increase corresponds to the difference in ionic radii between Br^- and I^-.

The number of halide ions and of water molecules in the two coordination spheres and in the remaining part of the solution, not involved in the coordination around erbium, can be estimated from the results given in Tables I–III. The values obtained are compared in Table IV with the stoichiometric compositions of the solutions and show that the water molecules are the preferred ligands in the first coordination sphere but the halide ions are concentrated in the second coordination sphere.

If the erbium halide solutions are described in terms of inner- and outer-sphere complexes, the diffraction measurements lead to the conclusion that inner-sphere complexes are formed only at very high ligand concentrations but outer-sphere complexes are extensively formed even at relatively low concentrations. The first coordination sphere of the erbium ion is occupied almost exclusively by water molecules. The halide ions are concentrated in the distinct second coordination sphere, where the halide:water ratio is larger than the stoichiometric ratio (Table IV).

Acknowledgment. Support from the Swedish Natural Science Research Council (NFR), from the foundation "Knut and Alice Wallenbergs Stiftelse", and from the Ministry of Education in Japan for H.Y. is gratefully acknowledged. We are indebted to E. Hansen and I. Desselberger for technical assistance.

Registry No. H_2O, 7732-18-5; $Er(ClO_4)_3$, 14017-55-1; $ErCl_3$, 10138-41-7; $ErBr_3$, 13536-73-7; Er, 7440-52-0; YCl_3, 10361-92-9.

Contribution from the Department of Chemistry and Materials Science Center, Cornell University, Ithaca, New York 14853-1301

Bonding in the Two-Dimensional Cu–Ga Layer of a Ca_2Cu_2Ga Crystal

Christian Kollmar and Roald Hoffmann*

Received September 7, 1989

We have examined the bonding properties of a two-dimensional layer containing linear Cu chains and unusual four-coordinate Ga atoms in a Ca_2Cu_2Ga crystal. The bond length between two Cu atoms bridged by two Ga atoms is slightly increased as compared to the bond length between two unbridged Cu atoms. We first calculated the band structure of a one-dimensional linear Cu chain and then introduced the Ga sublattice, thus forming the two-dimensional layer. The construction reveals how the bonding between the Ga-bridged Cu atoms vanishes almost completely, whereas the other Cu–Cu bond strength is not much affected. This is due to substantial mixing of Ga p orbitals into the symmetric intra-unit-cell linear combination of the Cu s orbitals in parts of the Brillouin zone, thus significantly weakening the Cu–Cu bond. For symmetry reasons, no such mixing is allowed for the antisymmetric linear combination of the Cu s orbitals. Introducing the Ca atoms to form the full three-dimensional structure has no major effect on Cu–Cu and Cu–Ga bonding but does place one partially filled Ca band in the valence region. Ca_2Cu_2Ga should be a conductor, unlikely to be subject to Peierls distortions. It should be possible to increase Cu–Ga bonding by feeding electrons into the Cu_2Ga sublattice.

Introduction

Recently, an investigation of the structure of some MCuGa compounds (M = Ca, Sr, Ba) has been published.[1] These compounds show unusual coordination geometries around Cu and Ga. For instance, one of them consists of linear Cu chains linked to two-dimensional layers through bridging Ga atoms. Linear metal chains are rare and so are the four-coordinate planar Ga atoms. The structure of this Ca_2Cu_2Ga compound is shown in **1**. The structural type is body centered orthorhombic, isotypic with Pr_2Ni_2Al.[2] **1** shows a three-dimensional view along the *a* axis of the crystal. The Ga atoms are represented by the hatched spheres, the Cu atoms by the smaller blank spheres, and the Ca atoms by the larger blank spheres. Since the distances between the Ca atoms and their nearest neighbors are larger than 3 Å, we neglect the corresponding Ca–Ga and Ca–Cu interactions in a first approach and treat the problem in two dimensions. The relevant two-dimensional slab of Cu_2Ga^{4-} is shown in **2**. It constitutes the *a*–*b* plane with the *b* axis oriented along the Cu chains.

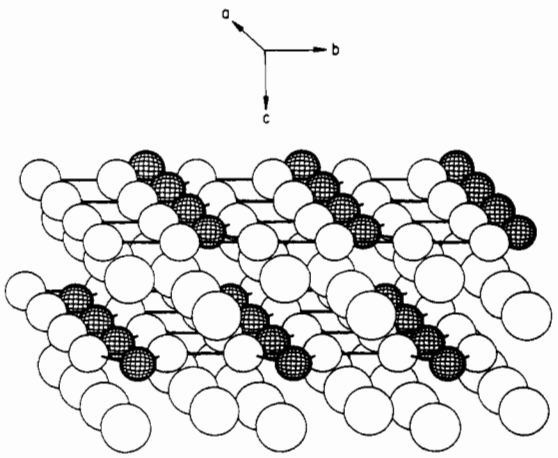

1

Note the linear Cu chains, nearly equally spaced at distances of 2.70 and 2.78 Å. The separations are longer than in Cu metal

(1) Fornasini, M. L.; Merlo, F. *J. Less-Common Met.* **1988**, *142*, 289.
(2) Rykhal, R. M.; Zarechnyuk, O. S.; Kuten, Ya. I. *Dopov. Akad. Nauk Ukr. RSR, Ser. A* **1978**, 1136.

0020-1669/90/1329-2466$02.50/0

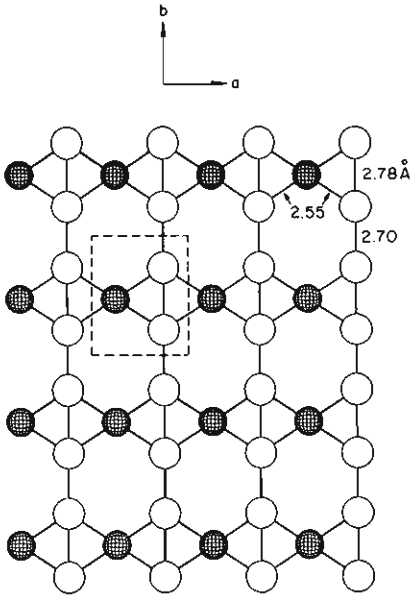

2

(2.55 Å).[3] At the same time, they are within the range of formally unbonded Cu^+ separations, which can be as short as 2.35 Å.[4] The bonding interactions between such Cu(I) centers, due to s–p mixing into the d^{10} shell, have been previously analyzed in this group.[5]

The one-dimensional Cu chains are linked by bridging Ga atoms. The distorted square-planar Ga coordination is unusual; we know of no counterpart in molecular compounds. Were the coppers formally in oxidation state I, then the Ga would be in oxidation state –VI, which is hardly likely. So the coppers must be reduced, at least formally. The electronic distribution in this slab, the unusual spacing of the coppers, and the geometry of the galliums, these are the subjects of our study.

We will proceed in three steps. First, we consider the Cu sublattice. Due to the large interchain separation, it is sufficient to restrict the calculation to a one-dimensional Cu chain. In a second step, we introduce the Ga atoms, thus forming the two-dimensional layer. In a final chapter, the effects of the interlayer Ca atoms on the band structure and bonding properties will be discussed. All calculations are done within the framework of a tight-binding version[6] of the extended Hückel theory[7] (see Appendix).

Band Structure of a One-Dimensional Cu Chain

The Cu–Cu distances in the two-dimensional layer are 2.70 and 2.78 Å, respectively. If one is looking for reasons for a bond length differential, it is useful to construct an idealized system with the relevant bond lengths equal and then look into the electronic structure, especially the overlap populations, for the origin of the differentiation. For this reason, we constructed an idealized lattice, with all Cu–Cu distances equal to 2.74 Å. To facilitate subsequent comparison with the two-dimensional layer, we choose two Cu atoms per unit cell. The resulting band structure is shown in Figure 1a and can be interpreted quite easily. Due to our choice of two atoms per unit cell, all the bands are folded back, resulting in a degeneracy at the edge of the Brillouin zone.[8] A representation of the bands at Γ and Y is shown in Figure 2. Please note the peculiar choice of representing the edge of the Brillouin zone by Y instead of X as is common practice for the one-dimensional case. This is due to the crystallographer's choice of the crystal axes for the three-dimensional structure.[1] They identify the Cu chain orientation with the b axis, which thus becomes the y direction. To avoid confusion with the choice of directions in the subsequently discussed two-dimensional case, we therefore have taken Y instead of X. We have numbered the bands in Figures 1 and 2. The group of ten bands located around –14 eV consists of d bands that show little dispersion and are not important in our case. The next two bands, 11 and 12, correspond mainly to the in-phase and out-of-phase linear combinations of the Cu s orbitals within the unit cell. At Γ they are of pure s character, whereas at other points in the Brillouin zone some mixing with the p orbitals oriented along the chain axis occurs (see e.g. ref 9). Since the energy separation between s and p orbitals is large as compared to the H_{ij} matrix elements of the s–p interaction, their mixing is not significant in our case. Nevertheless, it results in some additional bonding between the Cu atoms and a corresponding downshift in energy. Were the Cu atoms in oxidation state zero, then just the lower of the two bands would be occupied. The p bands are found at the top of Figure 1a. There are two degenerate π bands (13 and 14; 15 and 16) with small dispersion, which are formed by the p orbitals oriented perpendicular to the chain direction. The two wide p bands, 17 and 18, comprise p orbitals oriented along the chain direction. Except at Γ, they again are not pure p bands but mix with the s orbitals, now in an antibonding manner, causing an upshift in energy.

Linear one-dimensional chains are not that common; the reader might note, as a helpful reviewer did, the relationship of the Cu chain here with the P chain in NbPS.[10]

A useful indicator of bonding is the crystal orbital overlap population (COOP). This is an overlap population weighted density of states.[8] The Cu chain's COOP is shown in Figure 3a. Most of the bonding within the Cu chain is caused by the occupation of the lower, in-phase s band. The total overlap population amounts to 0.15 for neutral Cu. The mixing of the p orbitals into the s bands mentioned above is also reflected in Figure 3a. As can be seen quite easily, the total bonding in the s bands overrides the antibonding. If the bands were pure s, the situation would be reversed, because of the inclusion of overlap in the extended Hückel scheme.

Band Structure of the Two-Dimensional Layer

We now proceed to the two-dimensional Cu_2Ga layer, whose band structure is shown in Figure 1b. Again we have chosen an idealized lattice with equal Cu–Cu distances, in contrast to the real lattice with alternating distances. The Γ–X line in the Brillouin zone corresponds to a $\mathbf{k}$ vector parallel to the crystal a axis, i.e. the direction perpendicular to the Cu chains. The M–X region has to be compared to Figure 1a, for it is the k_y component that is changing there, as is the case in Figure 1a. To identify the bands, we have assigned numbers to them. Please note that this assignment is unambiguous only in the Γ–X–M region of the Brillouin zone. Due to avoided crossings, bands starting at a certain energy at Γ do not always terminate at the same point on the energy scale when returning to Γ from M.

Given that the d bands of Cu are almost not interacting, as may be seen from Figure 1b, we tried a simplification so as to facilitate the analysis of the essential Cu–Ga s–p orbital interactions. This was to drop the Cu 3d orbitals entirely out of the calculations. Figure 4 shows the resulting band structure of the Cu_2Ga two-dimensional layer. It can be seen by comparison with Figure 1b that it is mainly the lowest band (the Ga s band) which is affected. The interaction with the Cu d orbitals causes a downshift of ~0.5 eV in the X–M region. Corresponding to this effect, one of the

(3) Donohue, J. *The Structure of the Elements*; Robert E. Krieger Publishing Co.: Malabar, FL, 1982; p 220.
(4) Beck, J.; Strähle, J. *Angew. Chem., Int. Ed. Engl.* **1985**, *24*, 409.
(5) (a) Merz, K. M.; Hoffmann, R. *Inorg. Chem.* **1988**, *27*, 2120. (b) Mehrotra, P. K.; Hoffmann, R. *Inorg. Chem.* **1978**, *17*, 2187. (c) Dedieu, A.; Hoffmann, R. *J. Am. Chem. Soc.* **1978**, *100*, 2074.
(6) Whangbo, M.-H.; Hoffmann, R.; Woodward, R. B. *Proc. R. Soc. London, A* **1979**, *366*, 23.
(7) (a) Hoffmann, R. *J. Chem. Phys.* **1963**, *39*, 1397. (b) Hoffmann, R.; Lipscomb, W. N. *J. Chem. Phys.* **1962**, *36*, 2179.
(8) Hoffmann, R. *Solids and Surfaces: A Chemist's View of Bonding in Extended Structures*; VCH Publishers Inc.: New York, 1989; p 86.
(9) Burdett, J. K. *Prog. Solid State Chem.* **1984**, *15*, 173.
(10) Keszler, D. A.; Hoffmann, R. *J. Am. Chem. Soc.* **1987**, *109*, 118.
(11) Krieger-Beck, P.; Brodbeck, A.; Strähle, J. *Z. Naturforsch.* **1989**, *44B*, 237.

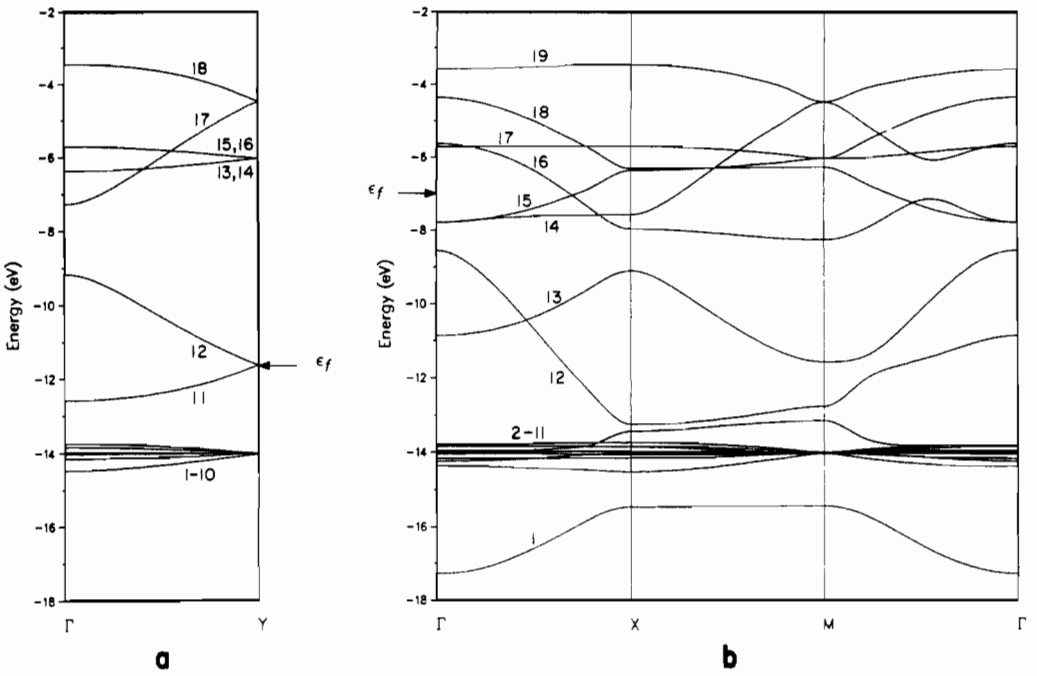

Figure 1. Band structure of a one-dimensional Cu chain with two atoms per unit cell (a) and the two-dimensional Cu_2Ga layer (b). The Cu–Cu distance is 2.74 Å in both cases. The x axis (Γ–X) and the y axis coincide with the a axis and the b axis of the crystal, respectively.

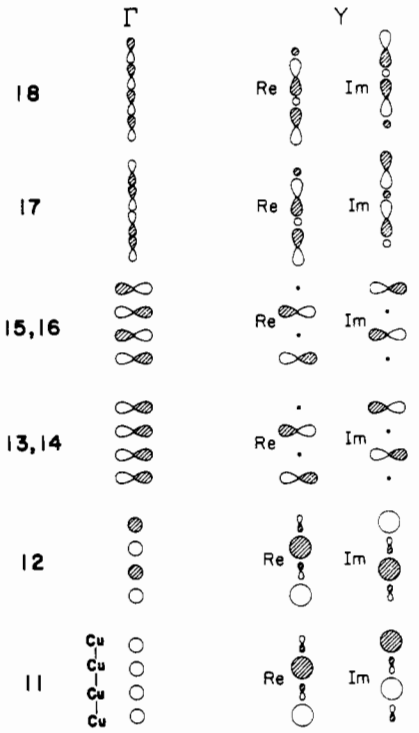

Figure 2. Orbital compositions of the bands 11–18 for the equidistant one-dimensional Cu chain. We have included two unit cells, i.e. four Cu atoms. At Y we show the real part (Re) and the imaginary part (Im) of the wave function.

Cu d bands (11) is upshifted (look at orbitals 1 and 11 in Figure 6). The remaining bands are not very much affected by interaction with the Cu d orbitals, some of them not at all for symmetry reasons, the others being only very slightly upshifted in energy. Thus, the essential features of the band structure are retained if the Cu d orbitals are omitted.

Note that the Fermi level crosses several bands. This material should be conducting (on this no experimental information is available, as far as we know). At the same time one needs to consider possible Peierls distortions, conceivably producing a gap in the Fermi level region. We will return to this later, but here let us proceed to a detailed analysis of the band structure of Cu_2Ga^{4-}.

The Ga orbitals appear with an energy of −14.58 (4s) and −6.75 (4p) eV. Since the p orbitals of Cu and Ga are of nearly the same energy, we would expect much interaction. This can be seen from Figure 5, indicating the Cu and Ga contributions to the total density of states (DOS). In Figure 5, for reasons just explained, we have omitted the Cu d orbitals completely. The mixing of Cu and Ga p orbitals occurs below the Fermi level in the region between −7 and −8 eV. The lower lying Ga and Cu s bands remain comparatively pure.

The orbitals corresponding to the bands at Γ, X, and M are shown in Figure 6. Looking at the band structure in Figure 1b between X and M, we recognize quite nicely some bands of the parent one-dimensional Cu chain. These are the bands 12 and 13, bands 15 and 17, and bands 14 and 19. The latter consist mainly of p orbitals pointing in the Cu chain direction and match nearly exactly their counterparts, bands 17 and 18, in the one-dimensional Cu chain. This is not surprising, because it can be seen from Figure 6 that there is only negligible Ga contribution to the orbitals of these bands. The same holds true for the narrow bands 15 and 17, which correspond to p orbitals perpendicular to the layer. Here, a mixing with Ga orbitals is not allowed for symmetry reasons.

Let us now look at bands 12 and 13 in some more detail. They correspond to in-phase and out-of-phase linear combinations of the Cu s orbitals. The out-of-phase band 13 again coincides with the corresponding band 12 of the one-dimensional chain. But, the in-phase linear combination band 12 in the two-dimensional case is stabilized considerably with respect to its one-dimensional counterpart band 11. As can be seen from Figure 6, this is due to a mixing with Ga p_x orbitals, which is symmetry allowed in the region X–M of the Brillouin zone. In contrast, the antibonding linear combination finds no Ga partner with the appropriate symmetry at X and M. This has important consequences, as we will see in the following.

We now look at the bonding situation in the two-dimensional network. The crystal orbital overlap population for the Cu–Cu bonds inside the unit cell (between Ga-bridged Cu atoms) and outside the unit cell is shown in Figure 3b. The total overlap population in the latter case amounts to 0.21 whereas in the former case the total overlap population has vanished almost completely (0.01). The observed bond length differential is less dramatic than this, only 0.08 Å. But the theoretical overlap population trend

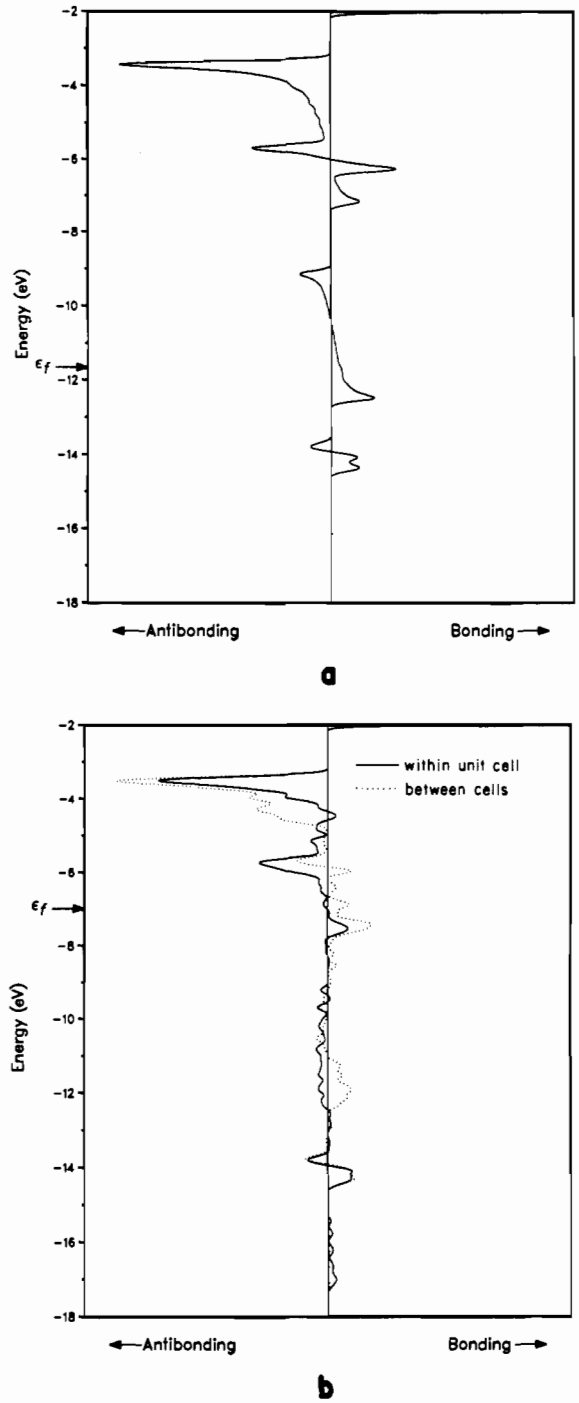

Figure 3. Crystal orbital overlap population of the Cu–Cu bonds for the one-dimensional Cu chain (a) and the two-dimensional Cu_2Ga layer (b). In the latter case we have to consider the Cu–Cu bonds within the unit cell (Ga-bridged Cu atoms) and between neighboring unit cells.

and observed bond length correlate.

Where does this difference come from? Looking at the COOP curve, we see that a difference between the two overlap populations arises primarily in the area around −12 eV, where they even have opposite signs. This is the area where the aforementioned bands 12 and 13 are located. Another hint is given by the projected density of states of the Cu s orbitals, which to a large degree is also located in that region. This can be seen from Figure 7. Consider the s bands 11 and 12 of the one-dimensional Cu chain, corresponding to bands 12 and 13 in the two-dimensional case. The in-phase Cu s band ranges from bonding at the zone center to nonbonding at the edge of the Brillouin zone, while the out-of-phase combination moves from antibonding at the zone center to nonbonding at the edge. Here, we have neglected the mixing with p orbitals, which, as already mentioned, results in additional

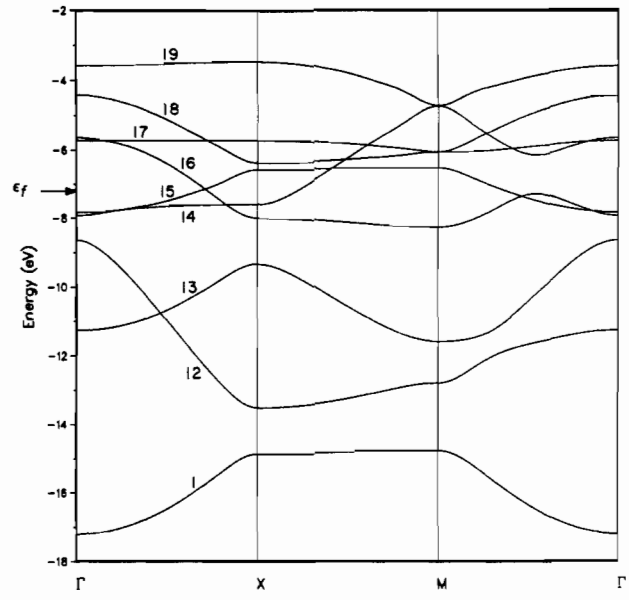

Figure 4. Band structure of the two-dimensional layer without the Cu d orbitals.

bonding. There clearly is no difference between inside- and outside-unit-cell bonding in this case, for we have chosen equal bond lengths.

Bringing in the Ga atoms changes the situation considerably. A gap opens between the two bands, due to stabilization of the lower one. This band is intracell bonding, but its bonding is diminished, simply because the coefficients of the Cu s orbitals are smaller in comparison to the s coefficients of band 13 due to mixing with the Ga p orbitals. On the other hand, the upper band retains its Cu–Cu antibonding properties, because contributions other than those of Cu s are negligible. It is interesting to note that even in this band, which has changed little in its energetic position or in its orbital composition, as compared to the one-dimensional Cu chain, considerable changes in the phase shifts of the orbital coefficients occur relative to the one-dimensional case. Now, near M, the upper band 13 is intracell antibonding and intercell bonding in contrast to its one-dimensional counterpart, which is intracell and intercell antibonding throughout the Brillouin zone. The lower band 12, however, is intracell bonding and intercell antibonding near M, whereas the corresponding one-dimensional band is intracell and intercell bonding throughout the Brillouin zone. This is reflected by the "bond order", a quantity given by the formula

$$p_{s_1 s_2} = c^*_{s_1} c_{s_2} + c_{s_1} c^*_{s_2}$$

The indices s_1 and s_2 refer to the Cu s orbitals. We have listed these bond orders for bands 12 and 13, at several points in the Brillouin zone, in Table I. The corresponding values for the one-dimensional Cu chain are also given in this table. When we compare the bond orders of band 13 with those of the corresponding band 12 in the one-dimensional case, it can be seen that they start with the same values at X. But as one moves toward M, the phase shift between the Cu s orbitals inside the unit cell is increased, and that outside the unit cell is decreased, in the two-dimensional layer as compared to the one-dimensional chain. As a consequence, band 13 as a whole is only slightly Cu–Cu antibonding outside the unit cell but largely Cu–Cu antibonding within the unit cell. In contrast, band 12 of the two-dimensional layer is largely Cu–Cu bonding inside the unit cell and only slightly bonding outside the unit cell. But the absolute numbers are much smaller now, due to the mixing with Ga p orbitals. This can be seen quite easily by comparing the bond order at X, where no phase shift occurs, with the corresponding value for the one-dimensional Cu chain. So the properties of band 13 prevail, leading to increased intercell and decreased intracell Cu–Cu bonding. The effect is even larger in the region of the avoided crossing between

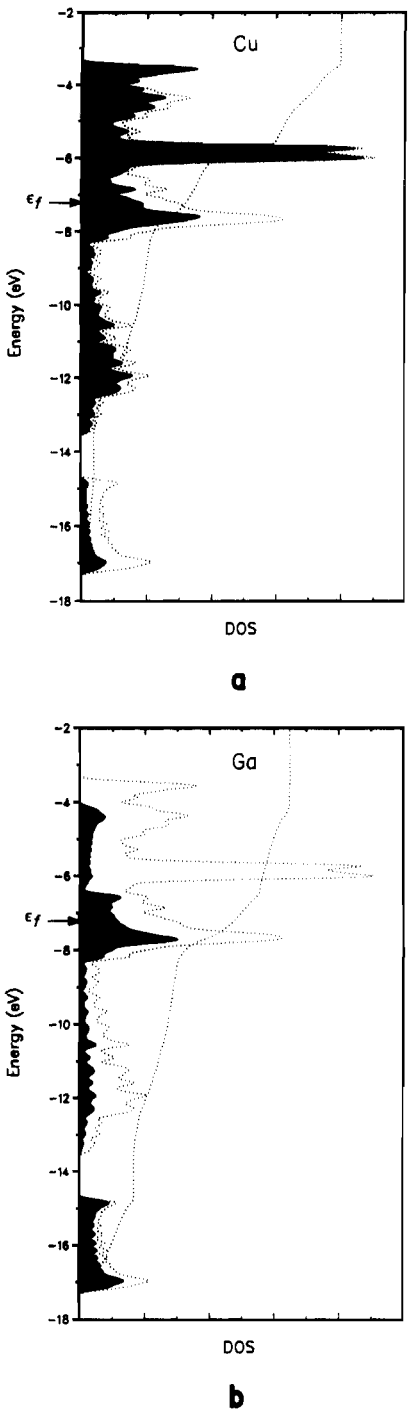

Figure 5. Contribution of Cu (a) and Ga (b) to the total density of states. The integration of the DOS is given by a broken line. Cu d orbitals are omitted in this calculation.

the two bands, along the line M–Γ in the Brillouin zone. As can be seen from Table I, both bands are intercell bonding and intracell antibonding in that area.

There clearly are other bands also contributing to Cu–Cu bonding, but the intercell–intracell difference arises mainly from bands 12 and 13, as argued above. Please note that there are large bonding and antibonding contributions to both Cu–Cu bonds just below and above the Fermi level, respectively. These bonds should therefore react sensitively to oxidation and reduction of the lattice. We will return to this. In contrast to our idealized lattice with equally spaced Cu atoms, the intracell Cu–Cu distance is larger by 0.08 Å than the intercell distance in the real lattice. This is not surprising, given our arguments above. The band structure and the bonding properties are not much affected by this small change.

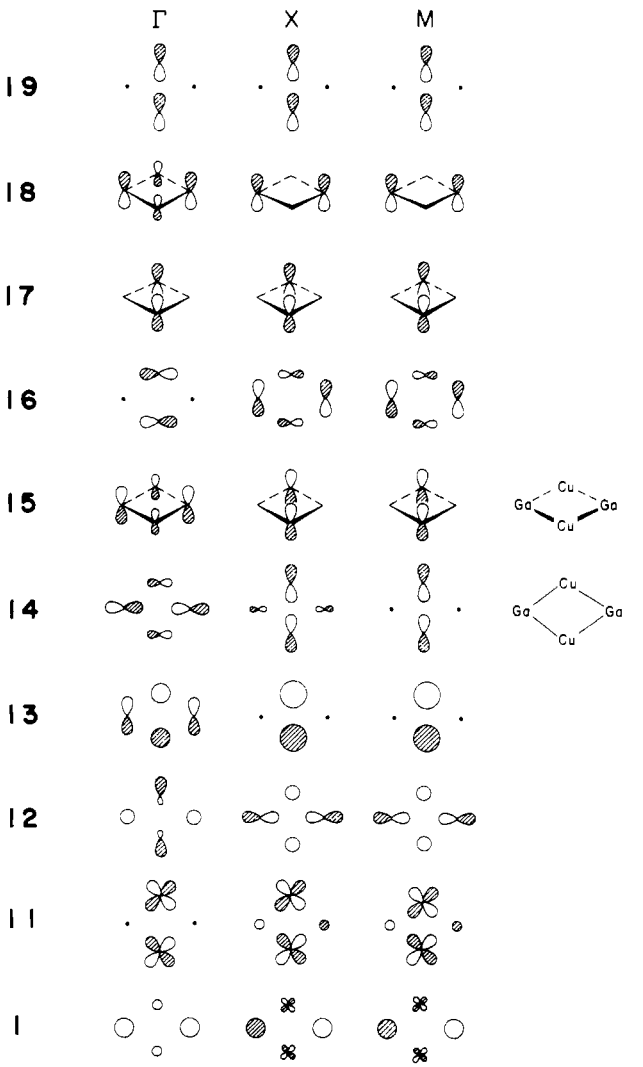

Figure 6. Orbital composition for the bands 1 and 11–19 at Γ, X, and M. The left and right atoms are Ga and the top and bottom atoms are Cu in each composed orbital. We have included one Ga atom of the neighboring unit cell. This allows us to see more clearly the symmetry type of the mixing orbitals. The orbitals 15, 17, and 18 consist of p_z orbitals oriented perpendicular to the layer.

Now let us examine the Cu–Ga bond in some more detail. As already mentioned, there should be considerable mixing of Cu and Ga p orbitals due to their close H_{ij}'s. This is actually the case, as can be seen from Figure 5. Whereas all the other contributions to the total DOS below the Fermi level can be attributed mainly to either Cu or Ga, the mixing occurs in the region between −7 and −8 eV. According to Figure 1b, bands 14, 15, and 16 are located in that energy range. Looking at Figure 6, we recognize quite nicely that the corresponding orbitals are mixtures of Cu and Ga p orbitals. This behavior is also reflected in the COOP curve of the Cu–Ga bond, which is shown in Figure 8. The highest bonding peak is located in the area between −7 and −8 eV, just below the Fermi level. So again there should be considerable sensitivity of this bond with respect to oxidation and reduction.

What happens if the layer is oxidized or reduced? The Cu and Ga charges, as well as the Cu–Ga and Cu–Cu overlap populations, for various oxidation states are given in Table II. It can be seen that large parts of the Cu–Cu and Cu–Ga bonding are lost on oxidation from −4 to −1 (the electron count changing from 29 to 26), corresponding to a shift in the Fermi level from −7 to −8 eV. We have already seen in the COOP curves of Figures 3 and 8 that large peaks of the Cu–Ga and Cu–Cu overlap populations are located in that energy range. On the other hand, the electron count of 29 of the Cu_2Ga^{4-} structure does not exhaust the bonding possibilities of our layer. The Cu–Ga and the inter-unit-cell

Table I. Bond Orders p of the Cu s orbitals for Intra- and Inter-Unit-Cell Cu–Cu Bonding at Several k Points and Corresponding Bond Orders of the One-Dimensional Cu Chain

	X				M				Γ
k_x	0.5	0.5	0.5	0.5	0.5	0.375	0.25	0.125	0.0
k_y	0.0	0.125	0.25	0.375	0.5	0.375	0.25	0.125	0.0
				2-D Cu_2Ga					
band 12 p(intra)	0.43	0.42	0.41	0.42	0.48	−0.09	0.15	0.21	0.29
band 12 p(inter)	0.43	0.39	0.24	−0.12	−0.48	0.38	−0.25	0.05	0.29
				1-D Cu					
band 11 p	0.78	0.73	0.58	0.32	0.0				
				2-D Cu_2Ga					
band 13 p(intra)	−1.23	−0.99	−0.86	−0.83	−0.87	−0.40	−0.54	−0.55	−0.57
band 13 p(inter)	−1.23	−0.74	−0.17	0.43	0.87	−0.05	0.28	−0.28	−0.57
				1-D Cu					
band 12 p	−1.22	−0.97	−0.66	−0.34	0.0				

Table II. Charge Distribution, Total Overlap Populations, and Fermi Level for Various Electron Counts

no. of electrons	charge			overlap population			
	total	Cu	Ga	Cu–Ga	Cu–Cu (intra)	Cu–Cu (inter)	E_F/eV
25	0	−0.4	0.8	0.338	−0.009	0.106	−9.75
26	−1	−0.75	0.5	0.393	−0.017	0.114	−8.02
27	−2	−1.0	0.0	0.462	−0.012	0.132	−7.67
28	−3	−1.3	−0.4	0.508	0.009	0.178	−7.44
29	−4	−1.6	−0.8	0.548	0.013	0.209	−6.99
30	−5	−2.0	−1.0	0.568	0.005	0.230	−6.50
31	−6	−2.3	−1.4	0.570	−0.019	0.241	−6.04
32	−7	−2.8	−1.4	0.569	−0.054	0.258	−5.89

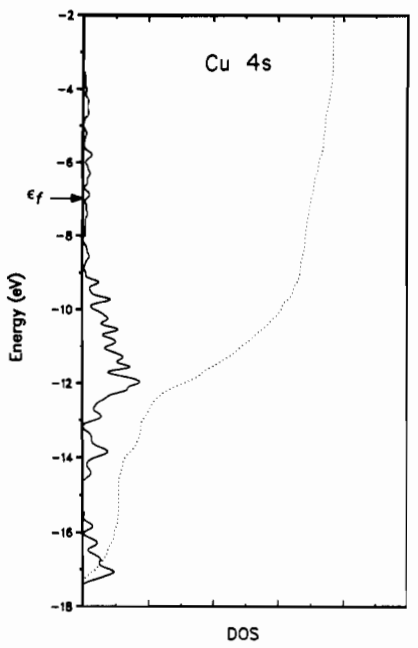

Figure 7. Projected DOS of the Cu s orbitals for the two-dimensional Cu_2Ga layer. The integral of the DOS is given by the broken line.

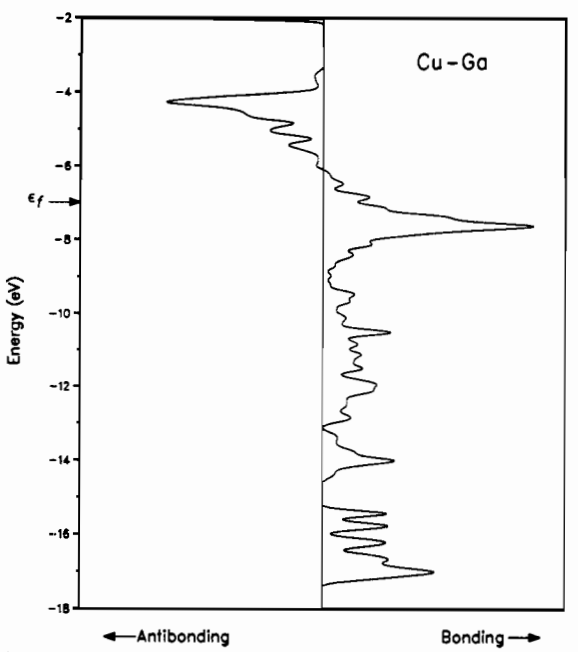

Figure 8. Crystal orbital overlap population of the Cu–Ga bond in the two-dimensional layer.

Cu–Cu overlap populations are further enhanced up to an electron count of 31 (Table II). We suggest that such reduced structures might be an interesting synthetic target.

Now we want to look at the charge distribution in the two-dimensional layer. As already mentioned, the Cu should be in a reduced state. When we look at the results of our calculation, each Cu carries a charge of −1.6, whereas the charge on Ga is −0.8. As can be seen from Figure 1, the Cu d bands and bands 12 and 13, which comprise mainly Cu s orbitals, are completely occupied. Figure 7 shows that ~70% of the Cu s states are occupied at the Fermi level. This contribution alone would account for a charge of −0.4 on each Cu atom. So there can be no doubt that Cu is in a reduced state. Let us now consider formally the Ga s band (1) and the Cu s bands (12 and 13) as completely occupied and localized on the indicated atoms. This can be justified from Figure 1. Then, we have Ga^+ and Cu^-. The remaining three electrons, which are necessary to account for a total charge of −4 per Cu_2Ga unit cell, are involved in covalent bonding through the aforementioned mixtures of Cu and Ga p orbitals just below the Fermi level (Figure 4). Distributing them evenly among the three atoms per unit cell would leave us with neutral Ga and Cu^{2-}. These considerations have to be taken with the caution appropriate to any oxidation state formalism. Table II shows us that our model of distributing the covalently bonding p electrons below the Fermi level evenly among the Cu and Ga atoms is actually not too bad. When the lattice is oxidized from −4 to −3 and −2, the charge shifts are 0.3 and 0.4 for Cu and Ga for each oxidation step, respectively.

Finally, we want to discuss the possibility of a Peierls distortion. The real structure already shows a slight distortion with respect to our idealized lattice, i.e. an alternation of the Cu–Cu bond length by ~0.08 Å. But that deformation does not open a gap

at the Fermi level. A real Peierls distortion is unlikely, due to the many bands crossing the Fermi level. Moving the Ga atoms is not promising because there is the almost pure Cu band 14 with its large bandwidth crossing the Fermi level. This band would hardly be affected by a dislocation of the Ga atoms. As we will see in the next section, there might even be an additional band with a strong Ca contribution appearing below the Fermi level, thus further decreasing the likelihood of a Peierls distortion.

As already mentioned, the structural type of Ca_2Cu_2Ga is analogous to that of Pr_2Ni_2Al.[2] It is interesting to note that the electron count of the Ni_2Al layer is exactly the same as in our Cu_2Ga layer. Since the charge of each Pr is 3+, the charge of the layer is 6- per Ni_2Al unit. Thus, the additional negative charge in Ni_2Al compensates exactly for the one electron each Ni lacks in comparison to Cu. In both cases we have a total electron count of 29 per unit of the layer (9 if we omit the 20 d electrons). There is another structure similar to ours, that is a K_2Au_3 compound.[11] Here, the group 3 element in the layer is replaced by another metal atom. Omitting the d orbitals, we have an electron count of 5 for the Au_3^{2-} sublattice, considerably less than the electron count of 9 for the previously described lattices. We will give an account of the electronic structure of this material in a future paper.

Qualitative Picture of the Bonding in Cu_2Ga^{4-}

From a chemist's standpoint, the Cu_2Ga^{4-} net in Ca_2Cu_2Ga is pretty unusual. It has linear copper chains and distorted square-planar galliums, both atypical geometrical features in molecular chemistry. We have seen the band structure of the layer, but how are we to understand simply the bonding within?

Let us begin as follows. If we omit the Cu 3d shell, we are left with 9 valence electrons per Cu_2Ga^{4-}, to be placed in combinations formed by 12 atomic orbitals. Looking at the band structure (Figure 1b or Figure 4), one can identify band 1 with Ga s and the lower part of bands 12 and 13 with inter-unit-cell Cu–Cu bonding, using both Cu s and p orbitals. A simplistic way to deal with this is to set up in-plane sp^2 hybrids at Cu and leave everything else unhybridized (**3**).

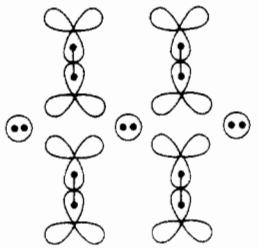

3

Now we have an s^2 lone pair on Ga and a Cu–Cu bond. That uses up four electrons of nine available per unit cell and three orbitals. Given similarities between Ga and B and between Cu and H, what comes to mind is electron-deficient three-center bonding[12] to describe the Ga–Cu interactions. In particular, an "open" three-center bond suggests itself (**4**). One could think

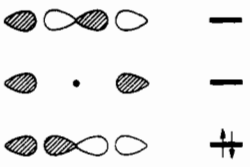

4

of each such three-center bond using one orbital and one electron from each Cu and one orbital and no electron from each Ga. Such three-center bonds crossing can be formed at each Ga. The bonding picture is reminiscent of that at the central B atom in B_5H_9[12] (**5**). The relevant delocalized combinations are com-

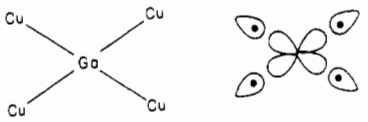

5

plicated, and not all are seen in Figure 6. Orbitals 14 and 16 do have important p_x and p_y contributions at Ga, at least in part of the Brillouin zone, and Cu–Ga bonding is concentrated in them.

This uses up four more electrons, leaving but one to be accounted for. This one enters one of the π bands formed from the p_z orbitals of Cu and Ga (bands 15, 17, and 18).

It is clear that the bonding in this two-dimensional net is very delocalized. A partially localized approach, as represented by the electron-deficient three-center bonding forwarded here, will catch only part of the essence of the bonding of this structure. But it is perhaps useful in making connections to structures and concepts in discrete molecular chemistry. The reader might relate this structure also to the well-known one of graphite, where a delocalized π system coexists with a localized (in graphite electron-sufficient, not electron-deficient) σ skeleton.

Band Structure of the Complete Three-Dimensional Lattice

So far, we have restricted our considerations to the two-dimensional layer. Thus, it is justified to ask about the role of the Ca atoms in the three-dimensional structure. Is there any significant bonding between them and the atoms of the layer? Looking at the short Cu–Ca distances of 3.06 and 3.09 Å and Ga–Ca distances of 3.26 and 3.47 Å, we cannot exclude this possibility in advance. The H_{ii}'s of Ca we take are -7 and -4 eV for the s and p orbitals, respectively. So the Ca s and the Cu and Ga p orbitals are close in energy, which also favors their mixing.

Before entering upon a detailed analysis of the three-dimensional band structure, we want to illustrate the position of the Ca atoms with respect to the two-dimensional layer, because this might not be apparent from **1**. **6** gives a view along the *c* axis of the crystal,

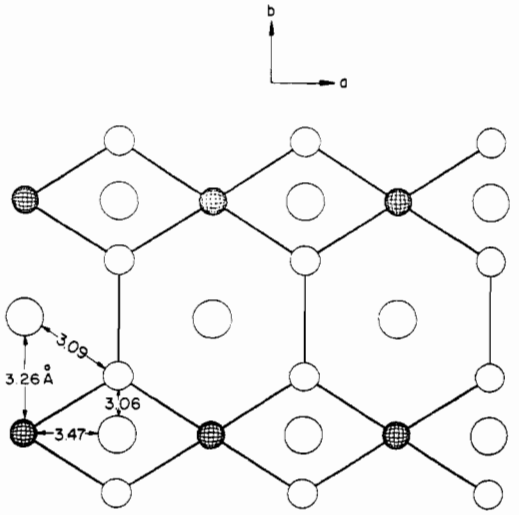

6

now with two Ca layers superimposed on the Cu_2Ga layer. The first Ca layer is located at a distance of 1.764 Å above the Cu_2Ga layer and consists of Ca atoms with the same *x* position as the Ga atoms. The Ca atoms of the second layer are located at a distance of 2.733 Å from the Cu_2Ga layer, just above the linear Cu chains. Please note that the Cu_2Ga plane is a symmetry plane

(12) Lipscomb, W. N. *Boron Hydrides*; W. A. Benjamin Inc.: New York, 1963.
(13) Canadell, E.; Eisenstein, O.; Rubio, J. *Organometallics* **1984**, *3*, 759.
(14) Hay, P. J.; Thibeault, J. C.; Hoffmann, R. *J. Am. Chem. Soc.* **1975**, *97*, 4884.
(15) Zheng, C.; Hoffmann, R. *J. Am. Chem. Soc.* **1986**, *108*, 3078.
(16) Ramirez, R.; Böhm, M. C. *Int. J. Quantum Chem.* **1986**, *30*, 391.

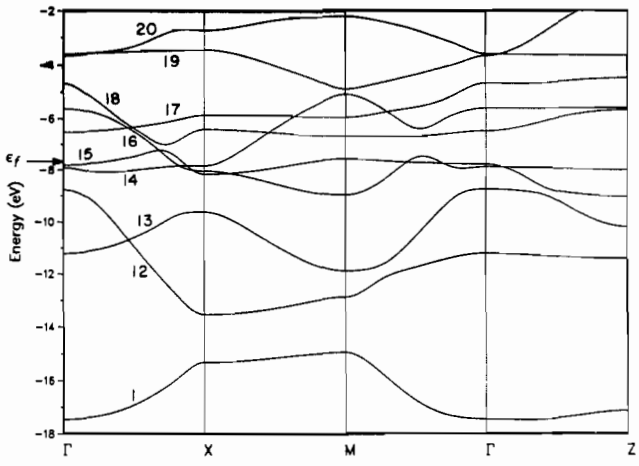

Figure 9. Band structure of the three-dimensional lattice along selected symmetry lines explained in the text.

of the crystal, so that there are corresponding Ca layers below it.

The band structure of the three-dimensional crystal is shown in Figure 9. We have again omitted the Cu d orbitals. Note that the assignment of the special points in the Brillouin zone has been chosen with respect to the corresponding two-dimensional lattice and, thus, does not coincide with the convention for the three-dimensional Brillouin zone of the body-centered orthorhombic lattice.[17] A cross section of this Brillouin zone in the k_x–k_y plane, with our choice of symmetry lines corresponding to Figure 9, is shown in **7**. Our points M and Z are identical with

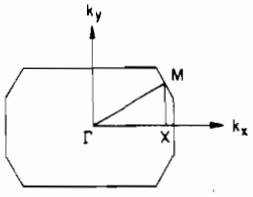

7

the points T and X, respectively, in the conventional notation.[17] The line Γ–Z is identical with the k_z direction, indicating a phase shift perpendicular to the layer.

Comparison of Figures 9 and 4 shows that there is only one additional band in the three-dimensional case (band 20) in our energy window. This seems surprising because the two Ca atoms add eight bands and their H_{ii}'s are located within the energy window. But even little mixing with lower lying orbitals is sufficient to strongly destabilize all but one of these Ca bands, so that they are not visible in Figure 9. Bands 1, 12, and 13 are very similar in Figures 4 and 9 over the whole Γ–X–M region. There is also no big difference in the energy values at Γ, except for band 17, which is downshifted by ~0.8 eV. But this is not important for us because this band is well above the Fermi level. Approaching X, some interesting changes occur. Band 18 "runs down" more strongly in the three-dimensional than in the two-dimensional case. Due to an avoided crossing, it ends up as band 15 at X. This band is now below the Fermi level and stays there for the most part of the X–M region, so that we have an additional band with strong Ca contribution below the Fermi level.

What do the orbitals of this band look like? From Figure 6 we know that band 18 is mainly the Ga p_z band. This band should be especially suited for an interaction with the Ca s orbitals, because the p_z orbitals are pointing out of plane and the energy match is also quite good. The orbital composition of band 15 (starting as band 18) at X is shown in **8**. Only the real part of the wave function is given. It may also be noted that band 16 experiences an additional downshift in the three-dimensional case

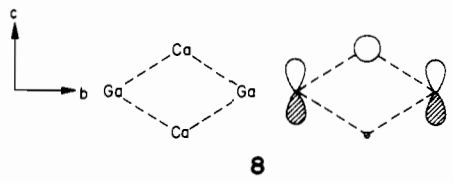

8

at M, of about 0.7 eV. This is also due to a bonding interaction with Ca. Figure 6 shows us that band 16 consists of a nice mixture of Ga p_y and Cu p_x orbitals. Again, they mix with the Ca s orbitals. The orbital composition illustrating the Ca–Ga and Ca–Cu bonding is shown in **9** and **10**, respectively.

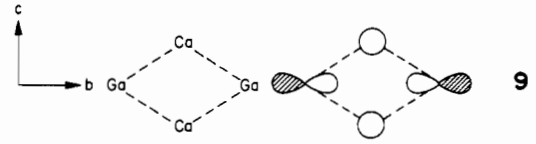

9

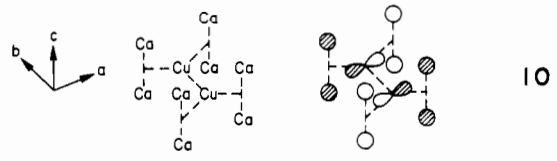

10

Now let us analyze the changes along the Γ–Z direction in the Brillouin zone. Considering the bands below the Fermi level, it is only band 15 that is significantly affected. There is an avoided crossing with the in-phase Cu s band. As can be seen from Figure 6, band 15 is a mixture of Ga and Cu p_z orbitals. The downshift is again caused by mixing with Ca s orbitals. The orbital composition for the Ca–Ga and Ca–Cu bonds is shown in **11**–**14**. It

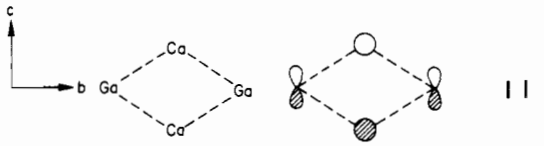

11

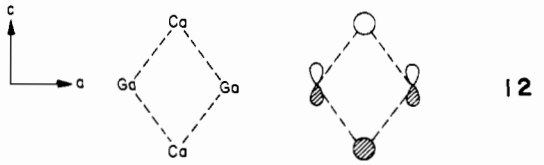

12

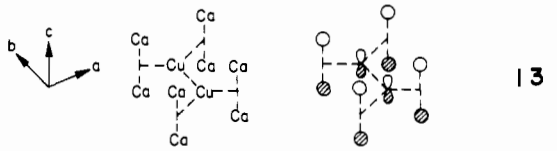

13

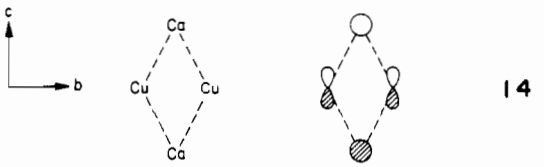

14

can be seen that all short Ca–Ga and Ca–Cu distances are now involved in the bonding interactions. Thus, it is not surprising that this favorable bonding situation results in a considerable downshift in energy of more than 2 eV for this band, as can be seen from Figure 9.

To make sure that we really have taken into account the most important interactions between the Ca atoms and the layer, we also have explored a different path in the Brillouin zone. This is one that still allows comparison with Figure 4 but, in contrast to the Γ–X–M part of Figure 9, includes some z component of

(17) Bradley, C. J.; Cracknell, A. P. *The Mathematical Theory of Symmetry in Solids*; Clarendon Press: Oxford, U.K., 1972; p 100.

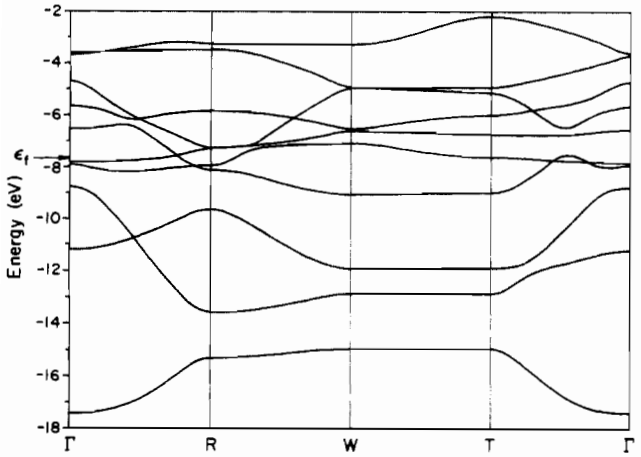

Figure 10. Band structure of the three-dimensional lattice for an alternative choice of symmetry lines.

the wave vector. The result is shown in Figure 10. Now we use the notation of ref 17 for the special points in the Brillouin zone, shown in **15**. The points X and M of Figure 4 correspond to R

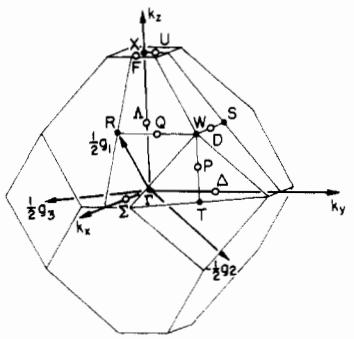

15

and W (or T), respectively, of Figure 10. The region between W and T in Figure 10 has no counterpart in Figure 4, for it is only the z component of the wave vector that changes here. Comparing Figures 4 and 10, we recognize that the band structures below the Fermi level are about the same in both cases. In contrast to Figure 9, no new band enters below the Fermi level. The only significant effect of the Ca atoms is again a stabilization of band 16 by an interaction analogous to **9** and **10**. In contrast to Figure 9, there is also no band below the Fermi level which is affected by a change of the z component of the wave vector, now occurring in the region between W and T. So our previous choice of k points in the Brillouin zone (**7** and Figure 9) seems quite reasonable and shows us the most important effects of the Ca atoms.

The interactions between the Ca atoms and the layer are not negligible. The overlap population for the shortest Ca–Ga contact of 3.26 Å (the corresponding orbital interactions are **8**, **9**, and **11**) amounts to 0.14, whereas the overlap population for the other short Ca–Ga distance, 3.47 Å (orbital interaction **12**), is slightly smaller (0.10). The overlap populations for the short Ca–Cu distances of 3.06 Å (orbital interaction **14**) and 3.09 Å (**10** and **13**) are 0.06 and 0.08, respectively. Their smaller magnitude may be due to the more contracted nature of the Cu orbitals. The Cu–Ga and the outside-unit-cell Cu–Cu overlap populations are 0.4 and 0.12, respectively, in the three-dimensional case. They are thus diminished with respect to the pure two-dimensional layer (0.54 and 0.21 for the Cu–Ga and Cu–Cu bonds, respectively). The electron density on each Ca atom amounts to ~0.7, with more than 60% of it in the Ca s orbital. Thus, less than 10% of the Ca states are occupied. This can also be seen from Figure 11, which shows the Ca contribution to the total DOS. Most of the Ca density below the Fermi level is located between −8 and −9 eV, arising from the interactions already discussed. The Fermi level is also downshifted by ~0.5 eV in the three-dimensional case.

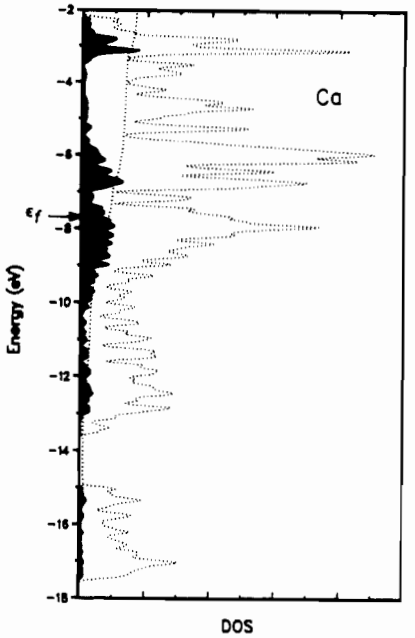

Figure 11. Contribution of Ca to the total DOS.

Table III. Extended Hückel Parameters[a]

atom	orbital	H_{ii}/eV	Slater exponents
Ga[13]	4s	−14.58	1.77
	4p	−6.75	1.55
Cu[14]	3d	−14.0	5.95 (0.5933), 2.30 (0.5744)
	4s	−11.4	2.2
	4p	−6.06	2.2
Ca[15]	4s	−7.0	1.2
	4p	−4.0	1.2

[a] The coefficients for the double-ζ expansion of the 3d orbitals are given in parentheses.

The important question, given the noticeable Ca mixing, is whether any of the conclusions we derived previously about Cu–Ga bonding are affected. They are not. The Cu–Cu and Cu–Ga COOP curves of the full three-dimensional structure (not shown here) are very similar to those illustrated above, even if the overall bonding is decreased.

Summarizing, we conclude that the Ca atoms play a more important role than that of a simple electron donor, even within our simple computational scheme. There is significant bonding between the Ca atoms and the atoms of the layer. Nevertheless, the pure two-dimensional layer remains a good approximation for evaluating Cu–Ga bonding. In general, molecular orbital calculations on Zintl phases and some intermetallic compounds have tended to neglect the alkali-metal, alkaline-earth-metal, or rare-earth-metal sublattices. Bonding with these has been often assumed to be purely ionic. It is worthwhile to check this assumption from time to time.

Summary

We have shown that the bonding properties of a two-dimensional Cu_2Ga layer in Ca_2Cu_2Ga can be analyzed most easily by decomposing it into its constituent Cu and Ga sublattices and subsequently considering the changes that arise from assembling the lattice. It turns out that the intracell Cu–Cu bonding has vanished almost completely whereas the intercell bonding is retained. This arises from a mixing of the bonding Cu s band with Ga p orbitals and accompanying phase shifts between the orbital coefficients. The main contributions to bonding in the layer arise from covalently bonding p electrons near the Fermi level. The compound should be metallic: it is unlikely to undergo Peierls distortions. The effects of oxidation and reduction on bonding have been traced, as well as the role of the Ca orbitals.

Acknowledgment. This work was made possible by a grant from the Deutsche Forschungsgemeinschaft and at Cornell was sup-

ported by NSF Research Grants CHE 8406119 and DMR 85-16616-A02.

Appendix

The tight-binding extended Hückel method was used for these calculations. A list of the parameters is given in Table III. The k point set used for the calculation of the average properties consists of 64 k points and was chosen according to the method of Ramirez and Böhm.[16]

Registry No. Ca_2Cu_2Ga, 118391-23-4.

Contribution from the Department of Chemistry and Biochemistry, University of Windsor, Windsor, Ontario, Canada N9B 3P4

Direct Electrochemical Synthesis of Copper and Silver Derivatives of Alkanedithiols and Crystal Structure of $[Cu_2S_2C_3H_6\text{-}1,2\cdot(C_6H_5)_2PCH_2P(C_6H_5)_2]_4\cdot 4CH_3CN$

Theodore A. Annan, Rajesh Kumar, and Dennis G. Tuck*

Received August 8, 1989

The electrochemical oxidation of copper or silver (=M) in acetonitrile solutions of $R(SH)_2$ (R = 1,2-C_2H_4, 1,2-C_3H_6, 1,3-C_3H_6, 1,4-C_4H_8, 2,3-C_4H_8, 1,5-C_5H_{10}, 1,6-C_6H_{12}) gives the insoluble homopolymeric M_2S_2R compounds in high yield. When $P(C_6H_5)_3$ or bis(diphenylphosphino)methane is present in the solution, the oxidation of copper yields adducts whose stoichiometry apparently depends on R. These results are discussed in terms of the possible structures involved. The compound $[Cu_2S_2C_3H_6\text{-}1,2\cdot(C_6H_5)_2PCH_2P(C_6H_5)_2]_4\cdot 4CH_3CN$ crystallizes in the triclinic centrosymmetric space group $P\bar{1}$ (No. 2) with a = 18.483 (7) Å, b = 11.673 (6) Å, c = 17.890 (7) Å, α = 116.57 (3)°, β = 111.35 (3)°, γ = 95.69 (3)°, V = 3052.08 Å^3, and Z = 2. Refinement converged at R = 0.0641 and R_w = 0.0657 for those 5727 reflections with $I > 3\sigma(I)$ and T = 20 °C. The molecule has a core Cu_4S_4 eight-membered ring, which is capped by six-membered Cu_3S_3 and Cu_2P_2CS rings and five-membered CuS_2C_2 rings.

Introduction

In a series of papers from this laboratory, we have described the synthesis of a variety of inorganic and organometallic compounds by a direct one-step method in which a metal is electrochemically oxidized in a nonaqueous solution of a ligand or a ligand precursor. Of particular relevance to the present work are those systems in which metal thiolates were obtained in high yield by oxidation in solutions of thiols or disulfides.[1-8] This technique provides a simple, high-yield, one-step route to thiolato derivatives of both main group and transition metals. We have also shown that analogous experiments with solutions of alkanedithiols, $R(SH)_2$, give rise to MS_2R species and their adducts, for M = Zn and Cd,[9] and to some unusual low-oxidation-state species for M = In.[10] Compounds of such ligands are of current biochemical importance, but also present some challenging structural problems, especially with d^{10} ions such as copper(I),[11,12] and the interest in the structure of copper(I) compounds has also been reinforced by their use in syntheses and as catalysts for hydrogenation and similar processes. We now report the preparation of a series of copper(I) and silver(I) derivatives of various alkanedithiols and, in the case of copper, some adducts with triphenylphosphine and 1,2-bis(diphenylphosphino)methane (dppm). The structure of the tetrameric dppm adduct of $Cu_2S_2C_3H_6$-1,2 involves a novel cage involving fused five-, six-, and eight-membered rings.

Experimental Section

General Data. Copper and silver anodes were in the form of rods, 6-mm diameter (Alfa Inorganics). Acetonitrile was distilled from calcium hydride and stored over molecular sieves. All other reagents were used as supplied (Aldrich).

Metal analysis was by atomic absorption spectrophotometry, using an IL-251 instrument, and microanalysis on selected compounds was performed by Guelph Chemical Laboratories Ltd. Infrared spectra were recorded on a Nicolet 5DX interferometer, using KBr disks.

Electrochemical Procedures. The electrochemical syntheses followed the methods described in earlier papers.[1-10] The cells were set up in 100-mL tall-form beakers and were of the general form

$$Pt_{(-)}/R(SH)_2 + CH_3CN\ (+L)/M_{(+)}$$

M = Cu, Ag L = PPh_3, dppm

and utilized solutions whose compositions are summarized in Table I. The high applied voltage required to drive the current (Table I) in such low-conductivity media was supplied by a Coutant LQ 50/50 power supply. The surface area of the anode exposed to the solution was ca. 6 cm^2. All the preparations were done under an atmosphere of dry nitrogen, which bubbled through the solution phase and thereby provided gentle stirring throughout the electrolysis.

As the reaction proceeded, hydrogen gas was formed at the cathode. The sequence of reaction, precipitation, etc. observed at the anode in the different systems is described below. We noted that with currents higher than those recorded, the surface of the anode tended to disintegrate, causing small particles of metal to contaminate any solid product formed in the cell.

Cu- and Ag/R(SH)$_2$. In all the systems studied, the product, which was subsequently identified as $M_2S_2(CH_2)_n$, began to precipitate in the cell almost as soon as the current flowed and continued to form throughout the electrolysis. The solid was collected by filtration, washed with acetonitrile (10–15 mL) and then diethyl ether (10–15 mL), and dried in vacuo. The compounds were characterized analytically (Table II); infrared spectroscopy confirmed the presence of the dithiolate ligand and also demonstrated the absence of the ν(S–H) vibration. Yields were typically 90–95%, based on metal dissolved.

Cu/$C_2H_4(SH)_2$-1,2/P(C_6H_5)$_3$. The product which precipitated during electrolysis under the conditions summarized in Table I was identified analytically as $Cu_2S_2C_2H_4$, and the infrared spectrum confirmed the absence of triphenylphosphine. No change in the composition of this precipitate was detected when the final reaction mixture obtained after 1 h of electrolysis was stirred vigorously for 1 h, but when the stirring was continued for 36 h at room temperature, the final product was $Cu_2S_2C_2H_4\cdot 4P(C_6H_5)_3$, in quantitative yield.

Cu/$C_3H_6(SH)_2$-1,2/P(C_6H_5)$_3$. Under the conditions shown in Table I, precipitation took place within ca. 5 min of the start of the electrolysis and continued throughout the experiment. The final reaction mixture was stirred vigorously for 1 h after the end of the electrolysis, and the

(1) Said, F. F.; Tuck, D. G. *Inorg. Chem. Acta* **1982**, *59*, 1.
(2) Hencher, J. L.; Khan, M. A.; Said, F. F.; Tuck, D. G. *Inorg. Nucl. Chem. Lett.* **1981**, *17*, 287.
(3) Hencher, J. L.; Khan, M. A.; Said, F. F.; Tuck, D. G. *Polyhedron* **1985**, *4*, 1263.
(4) Hencher, J. L.; Khan, M. A.; Said, F. F.; Sieler, R.; Tuck, D. G. *Inorg. Chem.* **1982**, *21*, 2787.
(5) Chadha, R. K.; Kumar, R.; Tuck, D. G. *Can. J. Chem.* **1987**, *65*, 1336.
(6) Khan, M. A.; Kumar, R.; Tuck, D. G. *Polyhedron* **1988**, *7*, 49.
(7) Chadha, R. K.; Kumar, R.; Lopez-Grado, J. R.; Tuck, D. G. *Can. J. Chem.* **1988**, *65*, 2151.
(8) Green, J. H.; Kumar, R.; Seudeal, N.; Tuck, D. G. *Inorg. Chem.* **1989**, *28*, 123.
(9) Mabrouk, H. E.; Tuck, D. G. *Inorg. Chim. Acta* **1988**, *145*, 237.
(10) Geloso, C.; Mabrouk, H. E.; Tuck, D. G. *J. Chem. Soc., Dalton Trans.* **1989**, 1759.
(11) Dance, I. G. *Polyhedron* **1986**, *5*, 1037.
(12) Blower, P. J.; Dilworth, J. R. *Coord. Chem. Rev.* **1987**, *76*, 121.

0020-1669/90/1329-2475$02.50/0